

## Suggesting a new testing device for determination of tensile strength of concrete

Hadi Haeri<sup>\*1</sup>, Vahab Sarfarazi<sup>2a</sup> and Ahmadreza Hedayat<sup>3b</sup>

<sup>1</sup>Young Researchers and Elite Club, Bafgh Branch, Islamic Azad University, Bafgh, Iran

<sup>2</sup>Department of Mining Engineering, Hamedan University of Technology, Hamedan, Iran

<sup>3</sup>Department of Civil and Environmental Engineering, Colorado School of Mines, Golden, Colorado 80401, USA

(Received February 27, 2016, Revised September 7, 2016, Accepted September 21, 2016)

**Abstract.** A compression to tensile load transforming (CTT) device was developed to determine indirect tensile strength of concrete material. Before CTT test, Particle flow code was used for the determination of the standard dimension of physical samples. Four numerical models with different dimensions were made and were subjected to tensile loading. The geometry of the model with ideal failure pattern was selected for physical sample preparation. A concrete slab with dimensions of 15×19×6 cm and a hole at its center was prepared and subjected to tensile loading using this special loading device. The ratio of hole diameter to sample width was 0.5. The samples were made from a mixture of water, fine sand and cement with a ratio of 1-0.5-1, respectively. A 30-ton hydraulic jack with a load cell applied compressive loading to CTT with the compressive pressure rate of 0.02 MPa per second. The compressive loading was converted to tensile stress on the sample because of the overall test design. A numerical modeling was also done to analyze the effect of the hole diameter on stress concentrations of the hole side along its horizontal axis to provide a suitable criterion for determining the real tensile strength of concrete. Concurrent with indirect tensile test, the Brazilian test was performed to compare the results from two methods and also to perform numerical calibration. The numerical modeling shows that the models have tensile failure in the sides of the hole along the horizontal axis before any failure under shear loading. Also the stress concentration at the edge of the hole was 1.4 times more than the applied stress registered by the machine. Experimental Results showed that, the indirect tensile strength was clearly lower than the Brazilian test strength.

**Keywords:** compression to tensile load convertor; tensile strength of concrete

### 1. Introduction

The tensile strength of concrete is a crucial design parameter in structures such as concrete dams, airfield runways, concrete roads and pavements, and other slabs. Therefore, many experimental and theoretical studies have been carried out to determine the tensile strength of

---

\*Corresponding author, Assistant Professor, E-mail: haerihadi@gmail.com

<sup>a</sup>Assistant Professor

<sup>b</sup>Assistant Professor

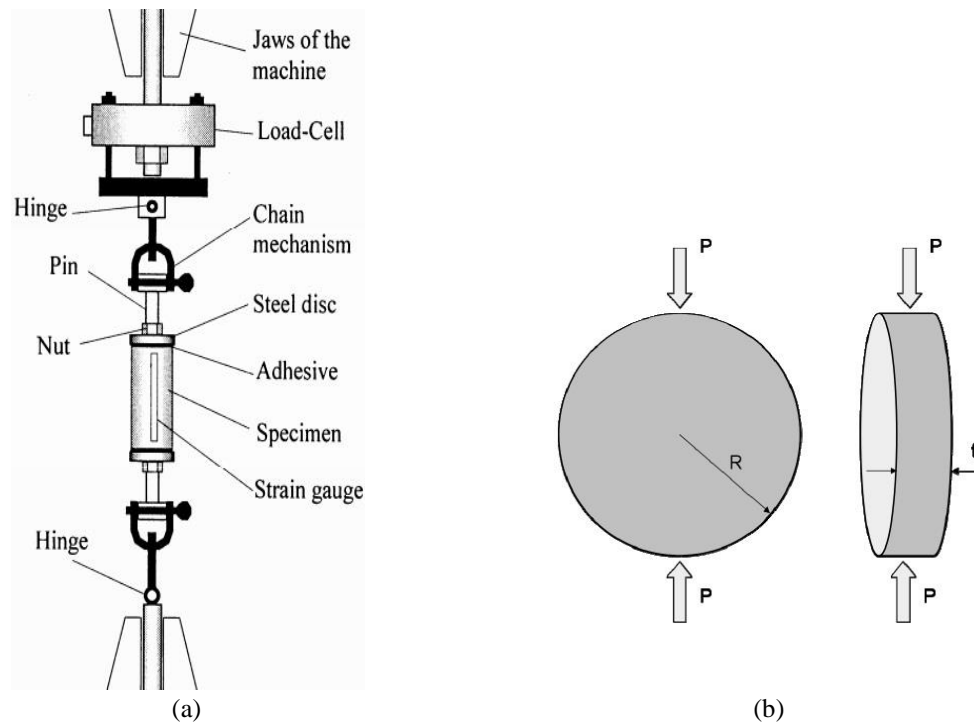


Fig. 1 (a) Specimen under uniaxial tensile loading, (b) Schematic of a splitting test for indirect measurement of tensile strength

concrete (Maso 1967, Luong 1990, Gomez 2001, Rocco, Guinea *et al.* 2001, Mier and Vliet 2002, Haeri 2011, Haeri and Ahranjani 2012, Haeri, Shahriar *et al.* 2013a, 2013b, 2014a, 2014b, Mobasher, Bakhshi *et al.* 2014, Kim and Taha 2014, Tiang, Shi *et al.* 2015, Wan Ibrahim, Hamzah *et al.* 2015, Silva, Brito *et al.* 2015, Gerges, Issa *et al.* 2015, Liu, Nie *et al.* 2015, Sarfarazi, Faridi *et al.* 2015, Haeri, Khaloo *et al.* 2015a, 2015b, 2015c, Haeri 2015d, 2015e, 2015f, Haeri and Sarfarazi 2016, Sardemir 2016). It is known that the stress obtained by breaking a specimen which is subjected to uniaxial loading, shows the real tensile strength of concrete (Fig. 1(a)). However, the tensile strength obtained from the uniaxial tensile test is more reliable than that of other test methods. But this test method requires much more care compared to indirect methods. Particularly, after the production of strong epoxy based adhesives, the uniaxial tensile tests are done with few troubles. Many experimental research were conducted in the past to determine the uniaxial tensile strength have failed because of unexpected crushing which occurred as a result of local stress concentrations. Another difficulty in uniaxial tensile tests is that the test specimen is under the influence of moment effects during the tensile test due to eccentricity.

The tensile strength of concrete can be obtained by indirect methods such as splitting test. The splitting tensile strength of a cylindrical sample with radius  $R$  and thickness  $t$  (as shown in Fig. 1(b)), is given as

$$\sigma_t = \frac{P_{max}}{\pi R t} \quad (1)$$

A non-uniform state of stress was superimposed over the local stress fluctuations that are caused by the material structure itself. Because of this, these methods have disadvantages (BS1881, 1983). Zhou (1988) reported that an increase in load eccentricity may decrease the tensile stress. Zain, Mahmud *et al.* (2002) proposed several equations that indicate the splitting tensile strength of high strength concretes based on the compressive strength of concretes of any age. Swaddiwudhipong, Lu *et al.* (2003) studied the strain capacity in direct tension and the tensile strength of concrete produced with different types of cement at early ages in their tests. The main objective of this paper was to develop a new loading device called compression-to-tension transformer for the determination of the tensile strength of the concrete specimen.

## 2. Numerical modeling

For determination of proper dimension of physical sample, firstly numerical simulation has been done using PFC2D. The models with different dimensions have been subjected to tensile loading and failure behavior has been studied. The geometry of model with tensile failure pattern was used as ideal geometry for experimental test.

### 2.1 Particle flow code3

Discrete element modeling (DEM) is now often used to simulate the behavior of rock (Potyondy and Cundall 2004). The method is attractive because it does not require the formulation of complex constitutive models. Particle flow code represents a rock mass as an assemblage of bonded rigid particles. In the two-dimensional version (PFC2D), circular disks are connected with cohesive and frictional bonds and confined with planar walls. The parallel bond model was adopted in this study to simulate the contacts between the particles. The values assigned to the strength bonds influence the macro strength of the sample and the nature of cracking and failure that occurs during loading. Friction is activated by specifying the coefficient of friction and is mobilized as long as particles stay in contact. Tensile cracks occur when the applied normal stress exceeds the specified normal bond strength. Shear cracks are generated as the applied shear stress surplus the specified shear bond strength either by rotation or by shearing of particles. The tensile strength at the contact immediately drops to zero after the bond breaks, while the shear strength decreases to the residual friction value (Itasca Consulting Group, Inc. 2004, Cho, Martin *et al.* 2007, Potyondy and Cundall 2004). For all these microscopic behaviors, PFC only requires the selection of the basic micro-parameters to describe contact and bond stiffness, bond strength and contact friction, but these micro-parameters should provide the macro-scale behavior of the material being modeled. The code uses an explicit finite difference scheme to solve the equation of force and motion, and hence one can readily track initiation and propagation of bond breakage (fracture formation) through the system (Potyondy and Cundall 2003). In addition, the user can track the failure process at each contact and determine if the dominant mode of failure is either tensile or shear. One of the requirements for the bonded particle model (BPM) is the calibration of the micro-contact parameters to match the macro-scale response.

#### 2.1.1 Brazilian test

The Brazilian test was used to calibrate the tensile strength of specimen in PFC2D model. Adopting the micro-properties listed in Table 1 and the standard calibration procedures (Potyondy

Table 1 Micro properties used to represent the intact rock

Parameter	Value	Parameter	Value
Type of particle	disc	Parallel bond radius multiplier	1
density	1000	Young modulus of parallel bond (GPa)	40
Minimum radius	0.27	Parallel bond stiffness ratio	1.7
Size ratio	1.56	Particle friction coefficient	0.4
Porosity ratio	0.08	Parallel bond normal strength, mean (MPa)	25
Damping coefficient	0.7	Parallel bond normal strength, SD (MPa)	2
Contact young modulus (GPa)	40	Parallel bond shear strength, mean (MPa)	25
Stiffness ratio	1.7	Parallel bond shear strength, SD (MPa)	2

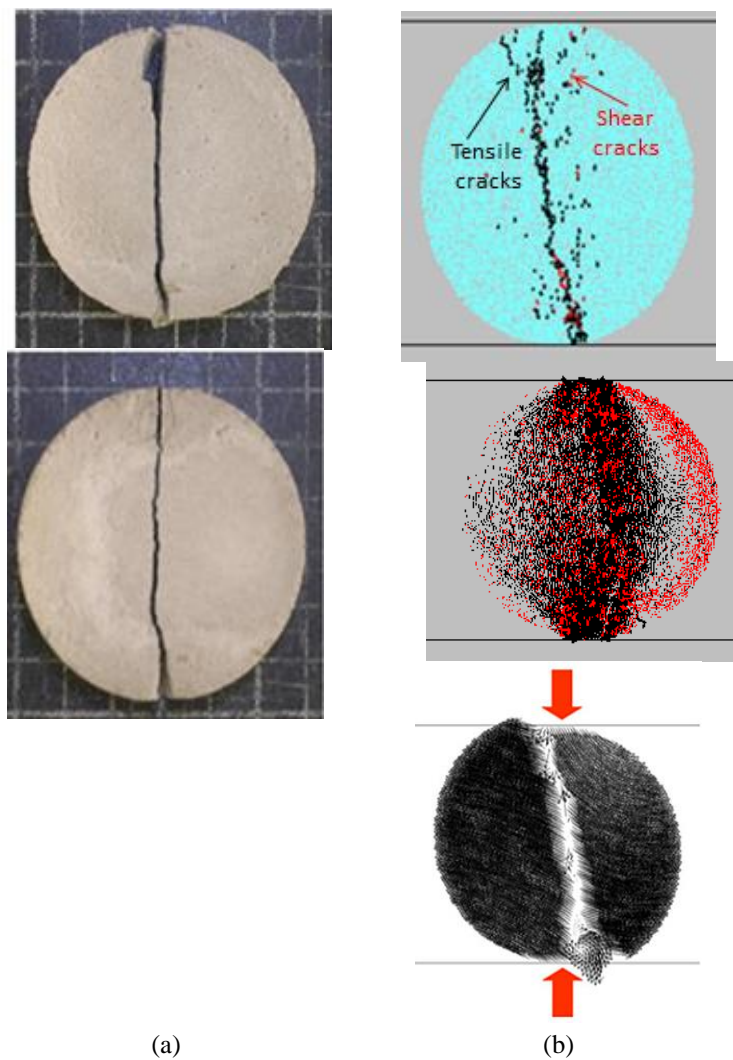


Fig. 2 failure pattern in (a) physical sample, (b) PFC2D model

Table 2 Brazilian tensile strengths obtained from physical and numerical tests.

Physical tensile strength (MPa)	4.5 and 4.7
Numerical tensile strength (MPa)	4.5

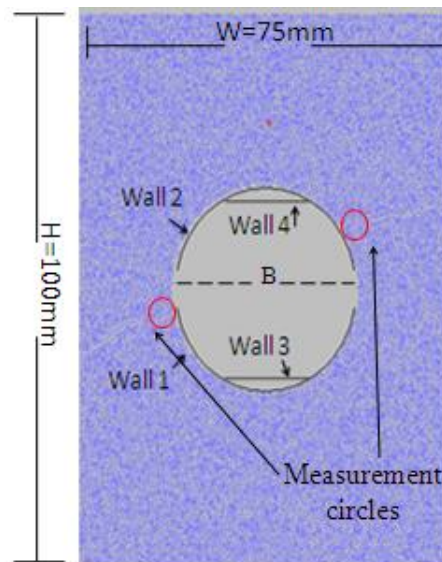


Fig. 3 Specification of numerical model

and Cundall 2003), a calibrated PFC particle assembly was created. The diameter of the Brazilian disk considered in the numerical tests was 54 mm. The specimen was made of 5,615 particles. The disk was crushed by the lateral walls moved toward each other with a low speed of 0.016 m/s. Fig. 2(a), (b) illustrate the failure patterns of the numerical and experimental tested samples, respectively. Also displacement vector of particle and bond force distribution was shown in Fig 2b. The failure planes observed in numerical and laboratory tests show a great agreement. The numerical tensile strength and a comparison of its experimental measurements were presented in Table 2. This table shows a good agreement between the numerical and experimental results.

### 2.1.2 Determination of proper dimension of physical sample using particle flow code

#### a) Preparing the model

After the calibration of PFC2D, indirect tensile tests were simulated by creating a box model in the PFC2D (by using the calibrated micro-parameters) (Fig. 3). The PFC specimen had the dimensions of 75×100 mm. A total of 11,179 disks with a minimum radius of 0.27 mm were used to make up the shear box specimen. A hole with diameter of B, was formed in the middle of model by deletion of particles from it. Models with four different ratios of hole diameter (B) to model width ( $W=75$  mm) of 0.125, 0.25, 0.375, and 0.5 were prepared. These models were subjected to internal tensile stress up to failure.

#### b) Loading set up

After model preparation, two semi-circle loading walls (walls 1 and 2) were installed in contact with the hole wall (Fig. 3). Also two horizontal walls (walls 3 and 4) with 2 cm of width were

placed in contact with the semi-circle walls (Fig. 3). Tensile loading was applied to the sample by moving the upper and lower walls in the positive side of Y-direction and in the opposite side of Y-direction, respectively. The wall velocity was adequately low (0.016 m/s) to ensure a quasi-static equilibrium. The Tensile force was registered by taking the reaction forces on the wall 3 in Fig. 3.

Two internal measurement circles were installed at the areas of crack initiation beside the hole. The diameter of this measuring circle was equal to the 1 cm (Fig. 3). The stress measurement circle was to evaluate how the tensile stress behaves during the tensile loading. Support of a PFC2D manual code was sought to measure the resulting contact force between the disks falling inside the circle. The tensile stress was a ratio of referred resulting contact normal force divided by the circle area.

### c) Tensile failure mechanism

Fig. 4(a)-(d) shows the progress of cracks in the models. Black lines and red lines represent the tensile cracks and shear cracks, respectively.

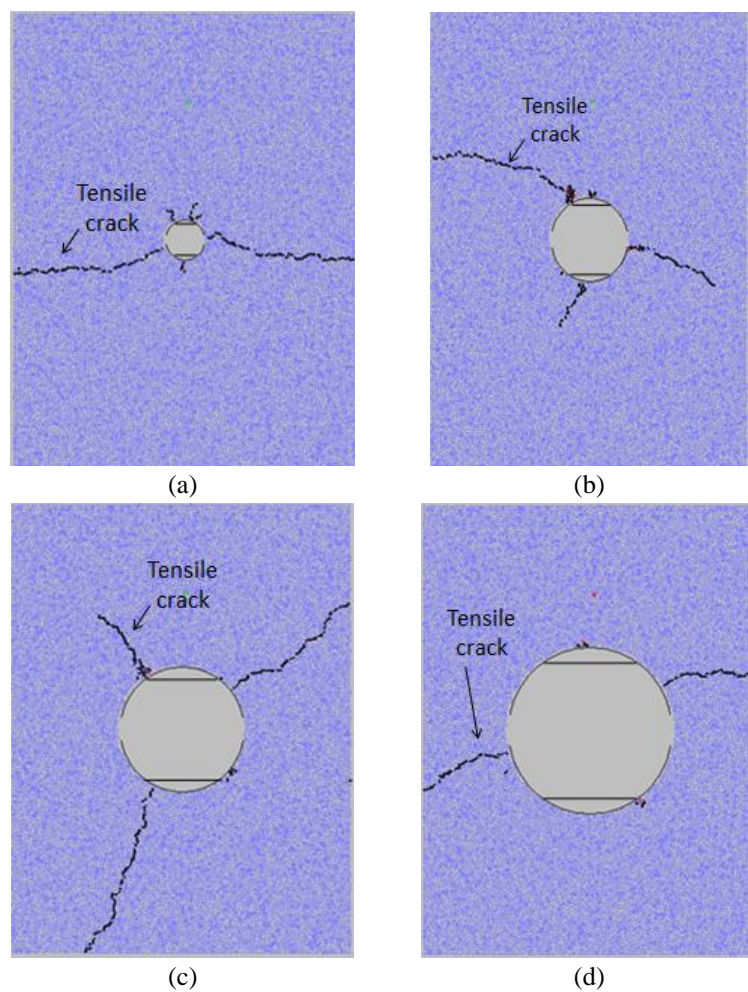


Fig. 4 Failure pattern in numerical model

When  $B/W=0.125$  (Fig. 4(a)), two tensile cracks initiate from both sides of the hole along the horizontal axes. These cracks propagate horizontally until they coalesce with the edge of the model. Several tensile cracks initiate from the top and bottom of the hole and propagate over a small distance.

When  $B/W=0.25$  (Fig. 4(b)), two tensile cracks initiate from top and bottom of the hole and propagate diagonally with respect to the loading axis. Also, one tensile fracture initiates from the left side of the hole and propagates diagonally with respect to the loading axis.

When  $B/W=0.375$  (Fig. 4(c)), two tensile cracks initiate from top of the hole and propagates diagonally with respect to the loading axis. The top left fracture coalesces with the edge of the model. Also, one tensile fracture initiates from bottom of the hole and propagates diagonally till it coalesces with the edge of the model.

When  $B/W=0.5$  (Fig. 4(c)), two tensile cracks initiate from both sides of the hole along the horizontal axes. These cracks propagates horizontally till coalesce with the edge of the model. It's to be noted that when  $B/W=0.5$ , the model splits into two separate blocks. These failure surfaces propagate nearly perpendicular to the tensile loading; therefore, it can be concluded that an ideal tensile failure occurred in the model. This ratio was chosen for experimental test on the concrete sample.

### 3. Experimental studies

A series of laboratory tests were performed to assess the performance of compression to tensile transformer, CTT, device to determine the indirect tensile strength of materials. Brazilian tension tests were also performed to compare the results with those of indirect tension tests.

#### 3.1 Compression-to-tensile load transforming device

A compression-to-tension load transformer device (CTT) was developed to determine the tensile strengths of specimens with a hole in the middle. This device converts the compression load to tensile load. The compression-to-tension load transformer device is comprised of four parts made from hardened stainless steel (Fig. 5). Part No. 1 is composed of two pieces as shown in Fig. 5(a). The front view of both pieces is "n" shaped and the side views look like "P" and "L" on the left and right, respectively (Fig. 5(a)). Part No. 2 is one piece and its front view is U shaped (Fig. 5(b)) and the side views look like "II". The dimensions of the pieces are shown in the Figure. Part No. 3 includes two semi cylindrical stainless steel sleeves, 7.5 cm in diameter, 6 cm long and 1 cm thick as shown in Fig. 5(c). Part No. 4 is composed of two similar steel blocks, 2 cm wide, 19 cm long and 1 cm thick (Fig. 5(d)).

#### 3.2 Test material and preparation technique of the specimens

The rock-like specimens were prepared from a mixture of two parts water, one part fine sand, and two parts of cement. The specimens were prepared by pouring slurry material in  $15 \times 19 \times 6$  cm containers, vibrated the containers to allow settling of the materials and then leave it to cure at room temperature for 8 hours. After the blocks were cured, a 7.5 cm diameter hole was bored through the center of each block (Fig. 6). According to numerical modeling results, the ratio of hole diameter to sample width was 0.5. Uniaxial compression and indirect tensile strengths of the

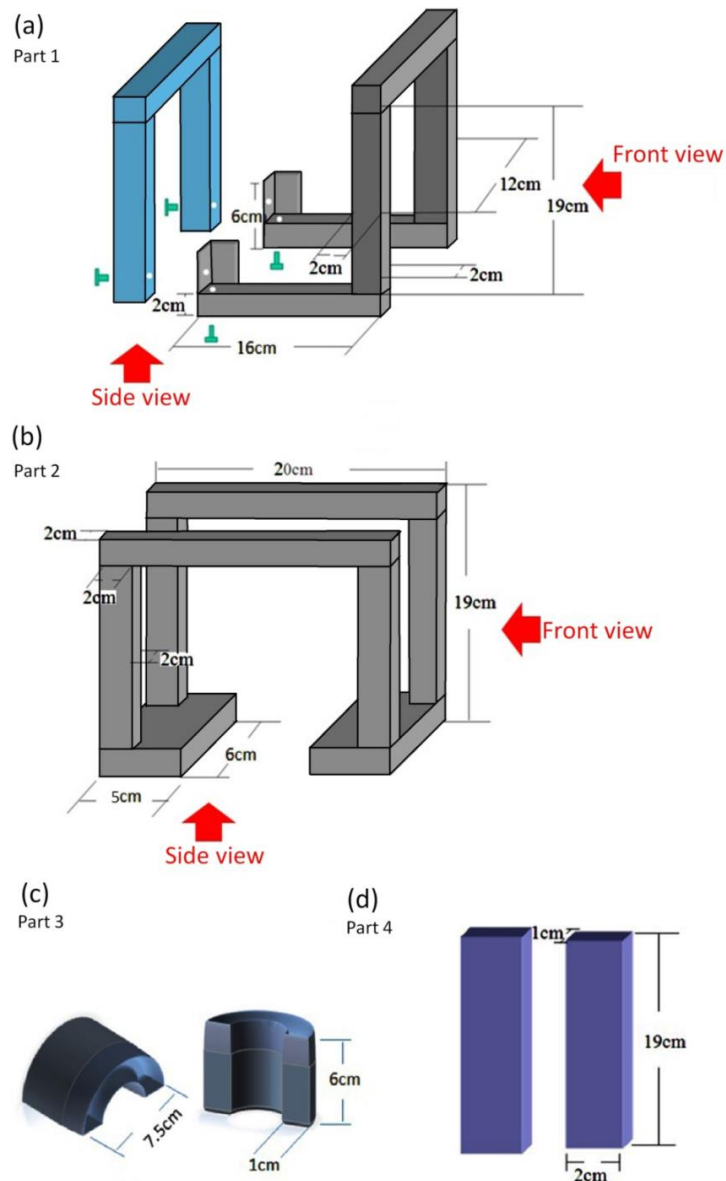


Fig. 5 Components of compression to tension converter device

intact material was also tested in order to control the variability of material.

Splitting test (BS1881, 1983) was also performed to compare the results with those of indirect tension test and in order to control the variability of material. The specimens for this test were 54 mm in diameter and 27 mm thick.

### 3.3 Installation of CCT device on the specimen

The set up procedure of CTT device consists of six stages, as shown in Fig 7. 1) The two

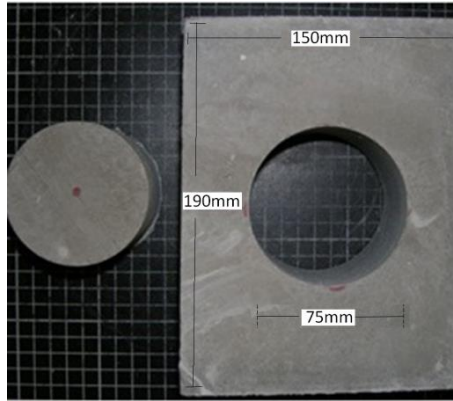


Fig. 6 The specimen prepared for CTT test

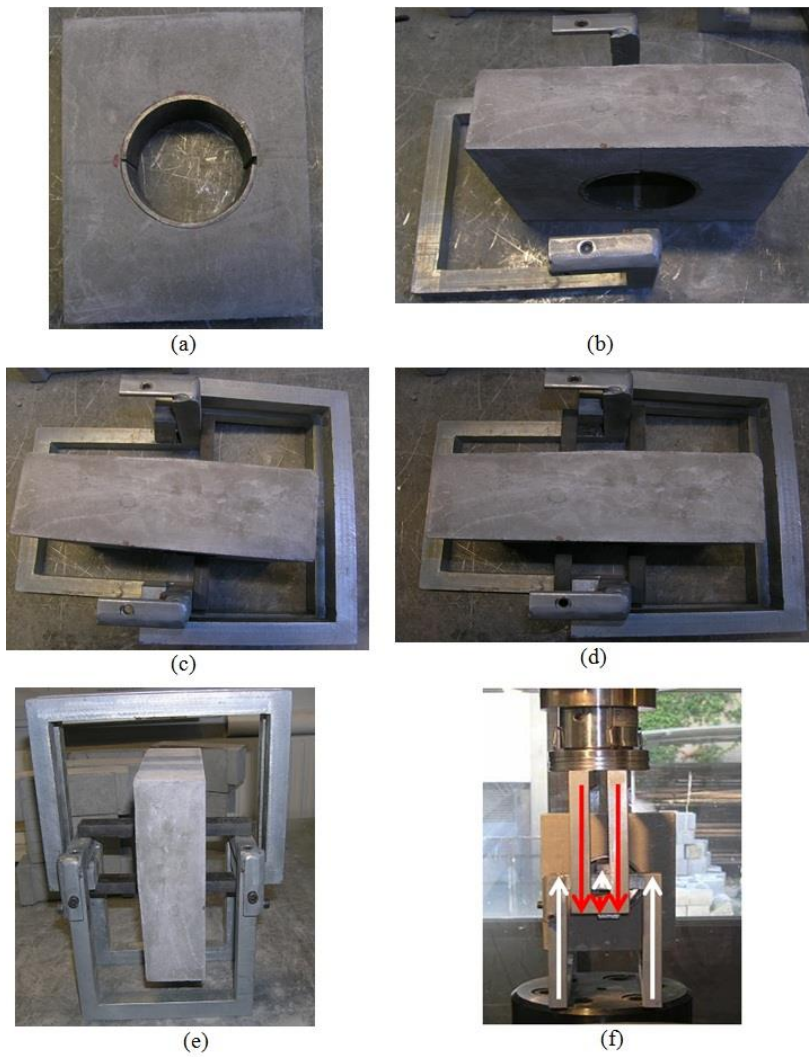


Fig. 7 The set up procedure of CTT device

stainless steel sleeves (Part No. 3) were inserted into the hole as shown in Fig. 7(a). 2) With the block laid vertically along its length, the “L” shape segment of Part No. 1 is placed on the left side of the specimen (Fig. 7(b)). 3) One of the steel blocks (Part no. 4) goes through the hole with its upper surface contacting the cylindrical sleeve and its lower surface contacting the “L” shape segment (Fig. 7(c)). 4) Part No. 2 is then placed on the right side of specimen (Fig. 7(c)).

5) The second steel block goes through the hole with its lower surface in contact with cylindrical sleeve and its upper surface contacts with the “II” shape segment, i.e., part number 2 (Fig. 7(d)). 6). The apparatus assembly is completed when the “T” shaped segment is screwed to the “L” shaped segment of Part No. 1, and the system is set in upright position (Fig. 7(e)). Under this assembly, the upper part of the concrete block (upper sleeve) is in contact with the lower part of the device and the lower part of the block (lower sleeve) is in contact with the upper part of the device (Fig. 7(e)). When the system is situated between the uniaxial loading frames (as shown In Fig. 7(f)), the upper loading frame compresses the steel sleeve against the lower part of the hole (i.e., pushes the lower part of the slab). Similarly, the lower loading frame pushes the steel block upward against the sleeve, which pushes up the upper part of block. The sample was subjected under tensile force as a resulting of applying the forces in opposite directions.

### 3.4 loading set up

A 30-ton compression loading machine applied compressive load to the CTT end plates (Fig. 8). An electronic load cell was used to measure the applied loading. The loading rate of 0.02 MPa/s was applied for all specimens. This rate was within the range recommended for the splitting testing. Three similar specimens were tested under tensile loading each test lasts for 3 minutes. All specimens tested using CTT cracked along a horizontal line through the center of the hole when subjected to a vertical force. The failure was a splitting tensile failure because the failure happened intentionally along the horizontal axis with the help of two sleeves (Fig. 9).

### 3.5 Experimental measurements

The two blades were in contact with the sleeves along their surfaces. Therefore, the tensile



Fig. 8 Compression load frame

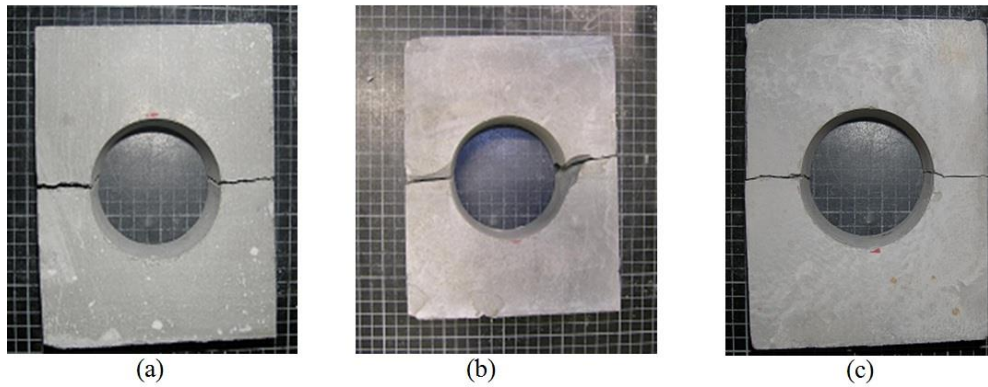


Fig. 9 The tensile failure pattern in samples

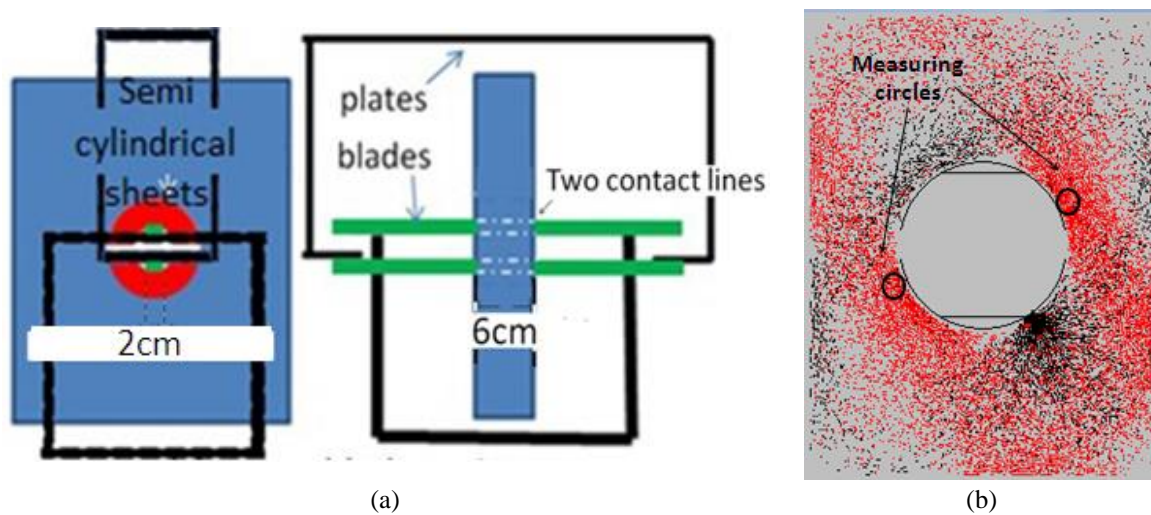


Fig. 10 (a) The blades in contact with the sleeves, (b) Bond force distribution in the model

loading on the slab was applied along the 2 cm×6 cm of the blade (Fig. 10).

For calculation of failure stress, the failure load registered by machine was divided to 12 cm<sup>2</sup>. According to the **Kirsch solution** (Brady and Brown 2006), the stress concentration at the edge of the hole along the horizontal axis is responsible for tensile failure. This concentration stress can be used as ultimate tensile strength of sample. Therefore, it should be to determine a relationship between tensile failure stress registered by machine and concentrated tensile stress at the edge of the hole should be determined.

### 3.6 Numerical simulation for determination of real tensile strength of concrete

Numerical simulation was necessary to determine a relationship between failure stress registered by data acquisition system and failure stress determined by measuring circle. Output of numerical simulation is a criterion which gives the real tensile strength of concrete. Fig 10b shows the bond force distribution in the model. Red and black lines represent the tensile force and

Table 3 Results of indirect tensile strength for  $W/B=0.5$  and Brazilian strength test

Sample No.	Experimental tensile strength (MPa)	Numerical tensile strength (MPa)	Brazilian tensile strength (MPa)
1	3.1	3.3	4.5
2	3.1	----	4.7
3	2.09	----	----
Average	3.03	3.3	4.6

compressive force, respectively. As can be seen, a pure tensile force has been observed in the measuring circle. When failure stress registered by data acquisition system was 2.3 MPa, the failure stress in measuring circle was 3.3 MPa. This means that stress concentration at the edge of the hole was 1.4 times more than applied stress on wall number 4 (Fig. 4). According to Kirsch solution, the failure stress concentration at the edge of the hole was equal to real tensile strength. Therefore the real tensile strength of concrete was determined by multiplying the failure stress on upper blade (Fig. 10(a)) or wall number 4 (Fig. 4) by 1.4. Based on this finding, Table 3 shows the real tensile strength of experimental and numerical simulation. Also the Brazilian tensile strength has been shown in the table.

### 3.7 Comparison of the strength results

Results from CTT and Brazilian test show that, both samples failed in tensile mode with smooth fracture surfaces. This could be justified through the observation of fracture path, perpendicular to applied tensile stresses. Investigating the fracture surfaces also showed that, both samples were separated in two pieces with no pulverization. Therefore, results from CTT and Brazilian test are comparable. Brazilian tension test yields the highest strength values (Table 3) due to high stress gradient along the incipient crack plane. Also, it is interesting to note that, the difference between the Brazilian and the indirect tensile strengths is about 33%. Difference in tensile strength from the two methods may therefore be partly governed by tensile stress distribution on the failure surface.

The tensile strength of experimental CTT test is nearly similar to the numerical one. The discrepancy between them is due to measuring circle diameter and its effect in tensile strength calculation.

## 4. Conclusions

The CTT device was designed to obtain an indirect tensile strength of concrete and to induce extension failure under a true uniaxial compression stress. Based on numerical modeling results, the best ratio of hole diameter to sample width for CTT test was 0.5. The hole diameter at the mid-section of specimen was 75mm. The model analysis shows that the failure under tensile loading occurs at the mid-length. No compressive stress exists at the mid-length of the models. The models fail under tensile loading before the failure by shear stress can occur at both ends of models. The results show that the tensile strength of experimental CTT test is similar to the numerical one. Also the indirect tensile strength was lower than the Brazilian tensile strength.

Finally, the proposed device was designed and fabricated for applications with commercially available compression loading machines. It is durable, inexpensive and easy to use. We believe the CTT can be used for testing brittle materials.

## References

- Brady, B.H.G and Brown, E.T. (2006), *Rock Mechanics for Underground Mining*, 3<sup>rd</sup> Edition, Chapman & Hall, London.
- BS1881-117 (1983), Testing Concrete-Method for determination of tensile splitting strength, British Standards Institute, London.
- Cho, N., Martin, C.D. and Segó, D.C. (2007), "A clumped particle model for rock", *Int. J. Rock Mech. Min. Sci.*, **44**, 997-1010
- Cho, N., Martin, C.D. and Segó, D.C. (2008), "Development of a shear zone in brittle rock subjected to direct shear", *Int. J. Rock Mech. Min. Sci.*, **45**, 1335-1346.
- Gerges, N., Issa, C. and Fawaz, S. (2015), "Effect of construction joints on the splitting tensile strength of concrete", *Case Stud. Constr. Mater.*, **3**, 83-91.
- Haeri, H. (2011), "Numerical modeling of the interaction between micro and macro cracks in the rock fracture mechanism using displacement discontinuity method", PhD Thesis, department of mining engineering, Science and Research branch, Islamic Azad University, Tehran, Iran.
- Haeri, H. (2015d), "Propagation mechanism of neighboring cracks in rock-like cylindrical specimens under uniaxial compression", *J. Min. Sci.*, **51**(3), 487-496.
- Haeri, H. (2015e), "Influence of the inclined edge notches on the shear-fracture behavior in edge-notched beam specimens", *Comput. Concrete*, **16**(4), 605-623,
- Haeri, H. (2015f), "Experimental crack analysis of rock-like CSCBD specimens using a higher order DDM", *Comput. Concrete*, **16**(6), 881-896.
- Haeri, H. and Ahranjani, A.K. (2012), "A fuzzy logic model to Predict crack propagation angle under disc cutters of TBM", *Int. J. Acad. Res.*, **4**(3), 156-169.
- Haeri, H. and Sarfarazi, V., (2016), "The effect of micro pore on the characteristics of crack tip plastic zone in concrete", *Comput. Concrete*, **17**(1), 107-112.
- Haeri, H., Khaloo, K. and Marji, M.F. (2015b), "Experimental and numerical analysis of Brazilian discs with multiple parallel cracks", *Arab. J. Geosci.*, **8**(8), 5897-5908
- Haeri, H., Marji, M. F. and Shahriar, K. (2015a), "Simulating the effect of disc erosion in TBM disc cutters by a semi-infinite DDM", *Arab. J. Geosci.*, **8**(6), 3915-3927.
- Haeri, H., Shahriar, K., Marji, M. F. and Moaref Vand, P. (2013b), "Simulating the bluntness of TBM disc cutters in rocks using displacement discontinuity method", *Proceedings of 13th International Conference on Fracture*, China.
- Haeri, H., Shahriar, K., Marji, M.F. and Moaref Vand, P. (2013a), "Modeling the propagation mechanism of two random micro cracks in rock samples under uniform tensile loading", *Proceedings of 13th International Conference on Fracture*, China.
- Haeri, H., Shahriar, K., Marji, M.F. and Moarefvand, P. (2014a), "On the cracks coalescence mechanism and cracks propagation paths in rock-like specimens containing pre-existing random cracks under compression", *J. Central South Univ.*, **21**(6), 2404-2414.
- Haeri, H., Shahriar, K., Marji, M.F. and Moarefvand, P. (2014b), "Investigating the fracturing process of rock-like Brazilian discs containing three parallel cracks under compressive line loading", *Streng. Mater.*, **46**(3), 133-148.
- Haeri, H., Shahriar, K., Marji, M.F. and Moarefvand, P. (2015c), "The HDD analysis of micro cracks initiation, propagation and coalescence in brittle substances", *Arab. J. Geosci.*, **8**, 2841-2852
- Itasca Consulting Group Inc, Particle flow code in 2-dimensions (PFC2D), Version 3.10, (2004) "Minneapolis. granite in tension with damage", *Theor. Appl. Fract. Mech.*, **36**, 37-49.

- Kim, J. and Taha, M.R. (2014), "Experimental and numerical evaluation of direct tension test for cylindrical concrete specimens", *Adv. Civil Eng.*, **2014**, Article ID 15692.
- Liu, X., Nie, Z., Wu, S. and Wang, C. (2015), "Self-monitoring application of conductive asphalt concrete under indirect tensile deformation", *Case Studi. Constr. Mater.*, **3**, 70-77.
- Luong, M. (1990), "Tensile and shear strengths of concrete and rock Tensile and shear strengths of concrete and rock Tensile and shear strengths of concrete and rock Tensile and shear strengths of concrete and rocktensile and shear strength of concrete and rock", *Eng. Fract. Mech.*, **35**(1-3), 127-135.
- Maso, J.C. (1967), "La nature minéralogique des agrégats facteur essentiel de la résistance des bétons a larupture et a l'action du gel", Ph.D. Thesis, University of Paul Sabatier, Toulouse, France.
- Mier, J.G.M. and Vliet, M.R.A. (2002), "Uniaxial tension test for the determination of fracture parameters of concrete", *Eng. Fract. Mech.*, **69**, 235-247.
- Mobasher, B., Bakhshi, M. and Barsby, C. (2014), "Backcalculation of residual tensile strength of regular and high performance fiber reinforced concrete from flexural tests", *Constr. Build. Mater.*, **70**, 243-253.
- Potyondy, D.O. and Cundall, P.A. (2004), "A bonded-particle model for rock", *Int. J. Rock Mech. Min. Sci.*, **41**(8), 1329-1364.
- Rocco, R., Guinea, G.V., Palans, J. and Elices, M. (2001), "Review of the splitting-test standads from a fracture mechanics point of view", *Cement Concrete Res.*, **31**(1), 73-82.
- Sardemir, M. (2016), "Empirical modeling of flexural and splitting tensile strengths of concrete containing fly ash by GEP", *Comput. Concrete*, **17**(4), 489-498.
- Sarfarazi, V. Faridi, H.R., Haeri, H. and Schubert, W. (2015), "A new approach for measurement of anisotropic tensile strength of concrete", *Adv. Concrete Construct.*, **3**(4), 269-284.
- Silva, R.V., Brito, J. and Dhir, R.K. (2015), "tensil strength behaviour of recycled aggregate concrete", *Constr. Build. Mater.*, **83**, 108-118.
- Swaddiwudhipong, S., Lu, H.R. and Wee, T.H. (2003), "Direct tension test", *Cement Concrete Res*, **33**, 2077-2084.
- Tiang, Y., Shi, S., Jia, K. and Hu, S. (2015), "Mechanical and dynamic properties of high strength concrete modified with lightweight aggregates presaturated polymer emulsion", *Constr. Build. Mater.*, **93**, 1151-1156.
- Wan Ibrahim, M.H., Hamzah, A.F., Jamaluddin, N., Ramadhansyah, P.J. and Fadzil, A.M. (2015), "Split Tensile Strength on Self-compacting Concrete Containing Coal Bottom Ash", *Procedia, Soc. Behav. Sci.*, **198**, 2280-2289.
- Zain, M.F.M, Mahmud, H.B, Ilham, A. and Faizal, M. (2002), "Prediction of splitting tensile strength of high-performance concrete", *Cement Concrete Res*, **32**, 1251-1257.
- Zhou, F.P. (1988), "Some aspects of tensile fracture behaviour and structural response of cementitious materials", Report TVBM-1008 Division of Building Materials, Lun Institue of Technology.